Geomechanics and Engineering, *Vol. 36, No. 3 (2024) 303-316*
https://doi.org/10.12989/gae.2024.36.3.303

Collapse failure mechanism of subway station under mainshock-aftershocks in the soft area

Zhen-Dong Cui*, Wen-Xiang Yan and Su-Yang Wang

State Key Laboratory for Geomechanics and Deep Underground Engineering, School of Mechanics and Civil Engineering, China University of Mining and Technology, Xuzhou, Jiangsu 221116, P.R. China

(*Received November 11, 2023, Revised January 6, 2024, Accepted January 15, 2024*)

Abstract. Seismic records are composed of mainshock and a series of aftershocks which often result in the incremental damage to underground structures and bring great challenges to the rescue of post-disaster and the repair of post-earthquake. In this paper, the repetition method was used to construct the mainshock-aftershocks sequence which was used as the input ground motion for the analysis of dynamic time history. Based on the Daikai station, the two-dimensional finite element model of soil-station was established to explore the failure process of station under different seismic precautionary intensities, and the concept of incremental damage of station was introduced to quantitatively analyze the damage condition of structure under the action of mainshock and two aftershocks. An arc rubber bearing was proposed for the shock absorption. With the arc rubber bearing, the mode of the traditional column end connection was changed from "fixed connection" to "hinged joint", and the ductility of the structure was significantly improved. The results show that the damage condition of the subway station is closely related to the magnitude of the mainshock. When the magnitude of the mainshock is low, the incremental damage to the structure caused by the subsequent aftershocks is little. When the magnitude of the mainshock is high, the subsequent aftershocks will cause serious incremental damage to the structure, and may even lead to the collapse of the station. The arc rubber bearing can reduce the damage to the station. The results can offer a reference for the seismic design of subway stations under the action of mainshock-aftershocks.

Keywords: collapse damage; earthquake resistance of underground structure; mainshock-aftershocks sequence; shock absorption; seismic precautionary intensity

1. Introduction

In recent years, the construction of underground structures has developed rapidly such as subway stations, underground shopping malls, underground tunnels, underground parking lots and so on. The development of urban underground space makes full use of space resources and provides great convenience for people's life. At the same time, the seismic performance of underground structures has also attracted many scholars' attention (Huynh *et al*. 2021, Kim *et al*. 2020, Kwon *et al*. 2020, Yoo *et al*. 2022). The seismic performance of underground structures was affected by the surrounding soil (Chou and Lin 2020, Cui *et al*. 2023a, Cui *et al*. 2023b, Kirkwood and Dashti 2018a, b, Sudevan *et al*. 2020). In the past, it was generally believed that the seismic performance of underground structures was better than that of above-ground structures (Tsinidis 2017, Xu *et al*. 2020b). However, in recent years, several strong earthquakes had caused great damage to underground structures, such as the Kobe earthquake in 1995, the Chi Chi earthquake in 1999 (Lu and Hwang 2018, Wang *et al*. 2001), the Wenchuan earthquake in 2008 (Wang *et al*. 2009) and the Chile earthquake in 2010 (Ruiz-Garcia 2012, Yin and Li 2011).

There are many researches on the seismic performance of underground structures, but most of them only focus on the mainshock. Geological survey shows that 89% of strong earthquakes are often accompanied by a series of aftershocks, and most of the aftershocks occur in a short time after the mainshock. Underground structures are at greater risk of damage in the mainshock-aftershocks. Therefore, there is an urgent need to solve the security problem of underground structures under the action of mainshock-aftershocks sequence.

At present, some scholars have carried out structural dynamic analysis under the action of mainshock-aftershocks. In 1894, Omori first began to study the mainshock-aftershocks sequence. According to the recorded aftershock data, the empirical formula of the attenuation of aftershock with time was obtained. Kim and Shin (2017) put forward a method to determine the amplitude and spectrum characteristics of aftershock records based on the mainshock records according to the NGA-West2 seismic wave database records.

In order to simplify the analysis process, the single-degree-of-freedom (SDOF) system was conducted to study the influence of mainshock-aftershocks on structural damage. Moustafa and Takewaki (2010) took the SDOF system as an example to analyze the influence of the mainshock-aftershocks sequence on the structural damage, and found that the mainshock-aftershocks sequence was more likely to cause damage to the structure than the

*Corresponding author, Professor
E-mail: cuizhendong@cumt.edu.cn

ISSN: 2005-307X (Print), 2092-6219 (Online)

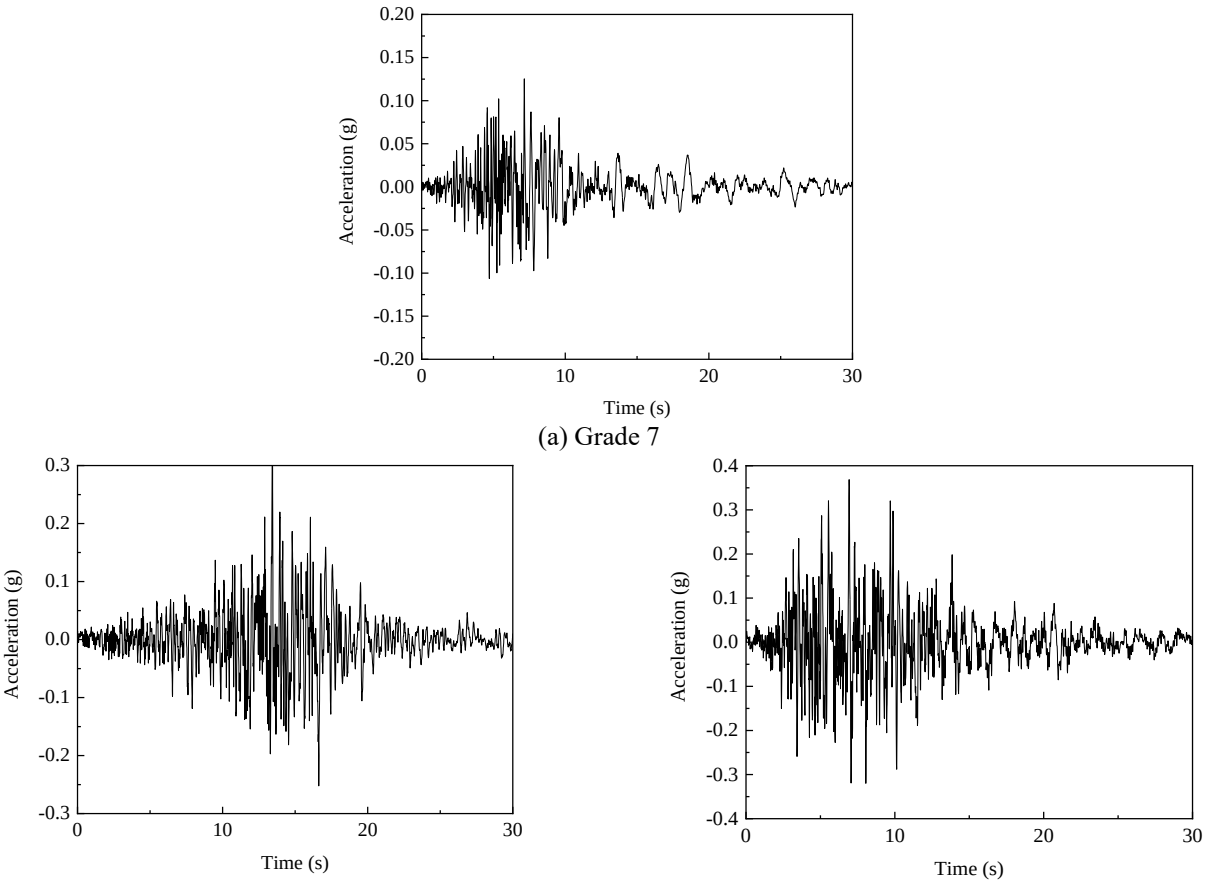

(a) Grade 7

(b) Grade 8

(c) Grade 9

Fig. 1 Seismic waves with different precautionary intensities

ordinary ground motion. Amadio *et al*. (2003) also found that the structural period and the characteristics of the mainshock-aftershocks sequence would make a great impact on the nonlinear time history response of the SDOF system. Although the aftershock significantly increased the incremental damage of the structure, the displacement response of the structure decreased significantly. However, few mainshock-aftershocks records were selected, and the influence of related parameters remained to be further analyzed.

The existing researches are mainly focus on the mainshock, but most of the earthquakes are a series of mainshock-aftershocks, which will aggravate the damage of the structure. Therefore, it is necessary to pay attention to the influence of mainshock-aftershocks sequence on the damage of underground structures, and put forward the corresponding anti-seismic countermeasures.

In this paper, the seismic waves with different seismic precautionary intensities were selected, and the mainshock-aftershocks sequence was conducted based on the repetition method for the dynamic time history analysis. Based on the Daikai station, the two-dimensional finite element model of the single-story two-bay subway station was established. According to the different seismic precautionary intensity, the dynamic response of the station under bidirectional coupling mainshock-aftershocks sequence was studied. The stress, displacement and inter-story drift ratio of the station were analyzed. The incremental damage ratio was introduced to quantitatively describe the incremental damage caused by aftershocks. The failure mechanism of the station under the mainshock-aftershocks sequence was investigated. The self-reset bearing damping technology was proposed and its reliability was verified by the numerical simulation.

2. Structure mainshock-aftershocks sequence

2.1 Seismic wave selection

The peak vertical design acceleration of the site should be 0.65 times of the peak horizontal design acceleration. The ratio of vertical to horizontal peak acceleration and the peak acceleration of basic ground motion of different seismic precautionary intensities are summarized in Table 1.

Several sets of seismic wave records of different seismic precautionary intensities are selected from the Pacific Earthquake Engineering Research Center (PEER), as shown in Table 2. Fig. 1 illustrates the acceleration time history curves. Three groups of seismic records are used to study the dynamic response analysis of underground structures under different seismic precautionary intensities. The "horizontal + vertical" bidirectional vibration is considered in the numerical simulation, where the vertical load is

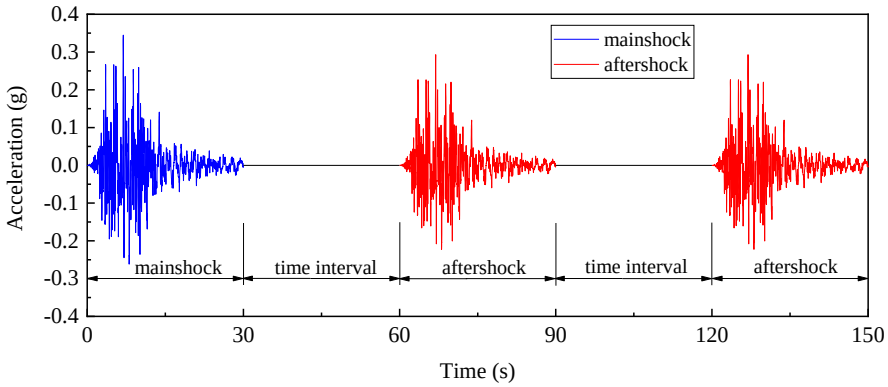

Fig. 2 Schematic diagram of mainshock-aftershocks sequence

Table 1 Ground motion parameters for underground structure design

Seismic precautionary intensity	7	8	9
Design acceleration (g)	0.15	0.3	0.4
Ratio of vertical to horizontal peak acceleration K_v	0.7	0.85	1
Peak acceleration of basic ground motion (g)	0.15	0.3	0.4

Table 2 Selective Wave Recording

Seismic precautionary intensity	Earthquake Name	Year	5~95% Duration (s)	Magnitude
Grade 7	Parkfield	1966	7.5	6.19
Grade 8	Darfield	2010	12.7	7.0
Grade 9	Kobe	1995	9.5	6.9

reduced according to the ratio of vertical to horizontal peak acceleration in Table 1.

2.3 Repetition method to construct mainshock-aftershocks sequence

In this paper, the repetition method (Hatzigeorgiou and Beskos 2009) was used to construct the mainshock-aftershocks sequence. This method assumes that the dynamic characteristics of the mainshock and the aftershocks are the same. Although this assumption is idealized, it is still widely used in the study of the mainshock-aftershocks sequence. The repetition method is to reduce the mainshock according to a certain functional relationship to construct one or more aftershocks, and then the complete mainshock-aftershocks sequence is used as the acceleration time history for dynamic analysis. When an earthquake occurs, there will be a series of aftershocks. In this paper, the analysis was simplified and only first two strong aftershocks were considered as the ground motion inputs. The PGA ratio of the aftershock to the mainshock was about 0.8526. In order to fully dissipate the inertial vibration produced by the mainshock, the time interval between the mainshock and the aftershock is set to 30 seconds (Yu *et al*. 2020). Fig. 2 illustrates the schematic diagram of the mainshock-aftershock sequence.

3. Numerical modelling

3.1 Finite element model

Daikai station was taken as an example to simulate the collapse process of underground structure. As shown in Fig. 3, the main part of the Daikai station is a one-story two-bay frame structure, 17.00 m in width and 7.17 m in height. The thickness of the top and bottom slab are 0.8 m and 0.85 m, respectively. The average reinforcement ratio is 1.0%. The thickness of the side wall is 0.7 m and the reinforcement ratio is 0.8%. The height of middle column is 3.82 m. The buried depth of the station is approximately 4.8 m. The width and depth of the finite element model are 100 m and 40 m, respectively. In the two-dimensional modeling, the middle column is regarded as a continuous wall, and the strength is reduced according to the actual three-dimensional section. Only the lateral seismic response of the subway station cross-section is considered in the numerical simulation model, which can be idealized as plane strain condition.

3.2 Constitutive model and boundary condition

The soil nonlinear behavior is described with the elastic-plastic model with Mohr-Coulomb failure criterion and the concrete is described with the concrete damaged plasticity model which reflects the damage mechanism of subsequent yield of concrete under periodic load by introducing damage factor *D*. The larger the damage factor is, the greater the damage degree of concrete is; the smaller the damage factor is, the smaller the damage degree of concrete is. The model can well simulate the law that the stiffness of concrete decreases with the increase of damage, and reasonably describe the mechanical behavior of concrete under reciprocating load. The soil parameters are summarized in Table 3 and the relevant parameters of concrete are summarized in Tables 4 and 5.

The soil and the structure of the station are discretized with 4-node element. The grid size of soil is 1 m. The normal contact between the underground structure and the soil is defined as “hard” contact. The tangential contact obeys Coulomb’s law of friction, and the friction coefficient of the contact surface is taken as 0.4. The steel bars are

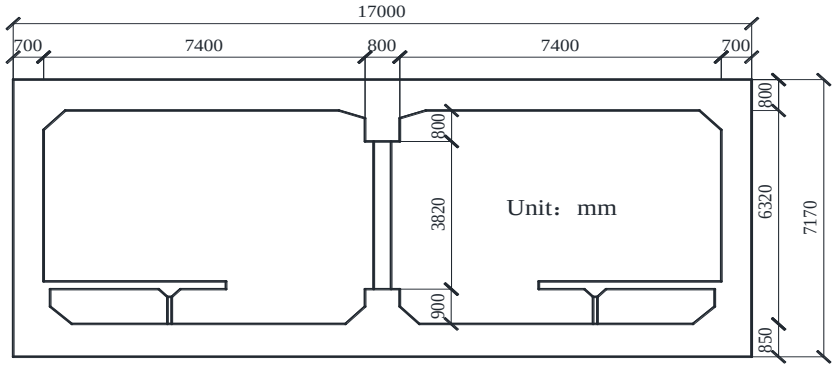

Fig. 3 Section dimension drawing of Daikai Metro Station

Table 3 Soil parameters

Soil type	Density (kg/m^3)	Initial shear wave velocity (m/s)	Shear modulus (MPa)	Damping ratio (%)	Poisson's ratio	Friction angle (°)	Cohesion (kPa)
sand	1960	140	8.09	18.63	0.3	34.5	0

Table 4 Parameters of C30 concrete

Compressive strength (MPa)	Inelastic strain (10^{-3})	Damage factor (d_c)	Tensile strength (MPa)	Inelastic strain (10^{-3})	Damage factor (d_t)
15.45	0	0	2.010	0	0
18.48	0.151	0.065	0.660	0.350	0.359
19.93	0.367	0.137	0.419	0.647	0.620
20.10	0.515	0.178	0.319	0.937	0.756
19.61	0.833	0.264	0.226	1.513	0.876
15.88	1.893	0.501	0.180	2.087	0.924
12.49	2.937	0.665	0.152	2.660	0.949
10.07	3.934	0.767	0.130	3.327	0.964
7.50	5.528	0.861	—	—	—
4.89	8.995	0.939	—	—	—

Table 5 CDP model parameters

Friction angle (°)	Dilation angle (°)	σ_{b0}/σ_{c0}	K	Viscosity parameter
38	0.1	1.16	0.6666667	0.0005

represented by truss elements and embedded into the structure. The nonlinear characteristics of the steel bar and the slip between the steel bar and the concrete are not considered.

A series of linear springs and viscous damper elements are set along the artificial boundary. The viscous damper simulates the radiation damping of the foundation, while the linear spring simulates the elastic restoring force of the foundation. It not only solves the problem of low frequency instability of viscous boundary, but also can simulate the elastic restoring force of foundation. Therefore, the viscoelastic artificial boundary has a good stability for both low frequency and high frequency.

3.3 Damping theory

Damping is a physical quantity used to characterize the energy dissipation performance of materials or structures. In this paper, it is assumed that the damping of the system mainly depends on the damping of the soil, and the damping characteristic of the soil mainly depends on the strain rate of the soil and has little to do with its response frequency. At present, Rayleigh damping (Xu *et al*. 2020a, Xu *et al*. 2019) is widely used in the material damping. Rayleigh damping assumes that the damping matrix of the structure is a linear combination of the mass matrix and the stiffness matrix, i.e.

$$[C]=\alpha[M]+\beta[K] \tag{1}$$

where α is the damping coefficient related to the mass matrix; β is the damping coefficient related to the stiffness matrix.

According to the orthogonal relationship between different vibration modes, the damping ratio of vibration modes ξ_n is expressed by α and β

$$\xi_n=\frac{\alpha}{2\omega_n}+\frac{\beta\omega_n}{2} \tag{2}$$

where ξ_n is the damping ratio of the nth mode shape; ω_n is the nth natural frequency of the system.

Table 6 First six natural frequencies of soil station model

Vibration mode	1st	2nd	3rd	4th	5th	6th
Frequency (Hz)	1.9495	2.4317	2.4605	2.0879	2.8957	3.0584

Table 7 Numerical simulation scheme

Working condition	Seismic precautionary intensity	Seismic wave	Loading mode	Ratio of vertical to horizontal peak acceleration K_v
1	7	Parkfield	Horizontal + Vertical	0.7
2	8	Darfield	Horizontal + Vertical	0.85
3	9	Kobe	Horizontal + Vertical	1

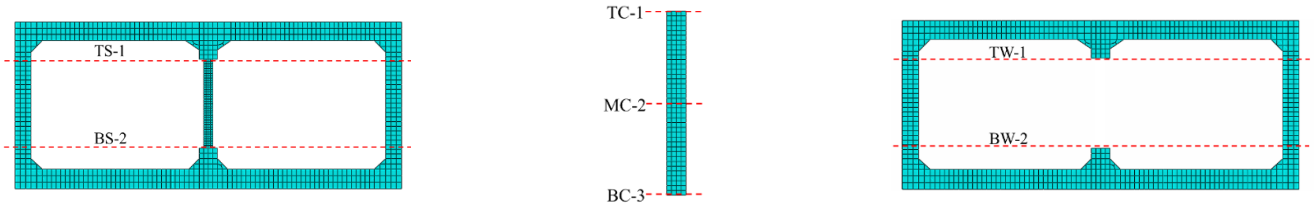

(a) Station (b) Middle column (c) Side wall

Fig. 4 Layout of monitoring section

Through the modal analysis, the first six natural frequencies of soil-structure are obtained, as shown in Table 6. Usually, the first two vibration modes make the greatest contribution. According to Rayleigh damping theory, the damping coefficient is obtained, α is 0.6799 and β is 0.0036.

4. Dynamic response analysis

According to different seismic precautionary intensities, the numerical simulation analysis of the station under the action of mainshock-aftershocks is divided into three groups, as shown in Table 7. The dynamic analysis is carried out according to the seismic waves selected in subsection 2.1. The mainshock-aftershocks sequence includes three stages: the mainshock, the first aftershock and the second aftershock.

In order to quantitatively analyze the change of the axial force of the station components, the key sections of the station, side wall and middle column are selected as the monitoring points, and the details are illustrated in Fig. 4.

4.1 Seismic precautionary intensity of Grade 7

The axial forces at the top and bottom of the station under seismic precautionary intensity of Grade 7 are marked in Figs. 5(a) and 5(b). In the static state before the earthquake, the middle column bears about 48% of the vertical load, and the side wall bears 52% of the vertical load. After the mainshock, the axial force of the station increases by 14%, but the increased axial force is mainly borne by the side wall, and the axial force of the middle column does not change much. The axial force of the middle column under seismic precautionary intensity of Grade 7 is marked in Fig. 5(c). The axial force at the top and bottom of the middle column is relatively large, while that in the middle is relatively small.

Fig. 6 illustrates the peak inter-story drift ratio and residual inter-story drift ratio of side wall with seismic precautionary intensity of Grade 7. The maximum peak inter-story drift ratio is in the mainshock, about 0.0021. In the three stages of the mainshock-aftershocks, the residual drift ratio increases gradually, and the maximum residual inter-story drift ratio is in the second aftershock, about 0.0007. Under the seismic precautionary intensity of Grade 7, the top and bottom of the middle column and the bottom of the side wall are slightly damaged after the mainshock, but the two aftershocks do not cause incremental damage to the structure.

4.2 Seismic precautionary intensity of Grade 8

Fig. 7 illustrates the peak inter-story drift ratio and residual inter-story drift ratio of side wall with the seismic precautionary intensity of Grade 8. The axial force of the station increases significantly after the mainshock. It is mainly due to the shear failure of the overlying soil, which significantly increases the vertical load of the ceiling and further leads to the decrease of the horizontal deformation capacity. However, this part of the load is mainly borne by the side wall and do not increase the axial force of the middle column, which is the same as the result under the seismic precautionary intensity of Grade 7. After the mainshock, the axial force of the side wall is about double that of the static state. However, the subsequent two aftershocks have little influence on the axial force of the station, indicating that the shear failure of the soil mainly occurs in the stage of the mainshock.

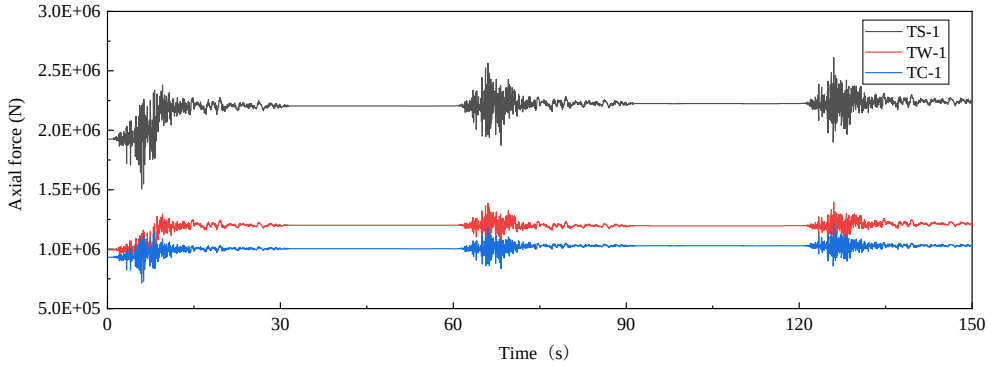

(a) Top of station

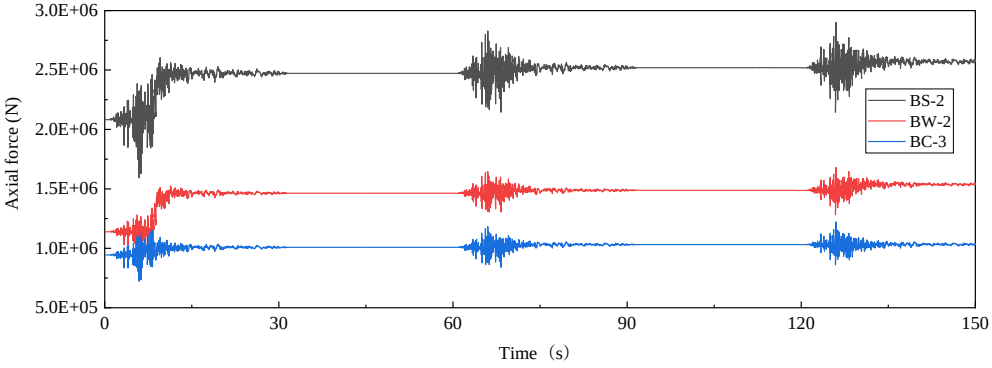

(b) Bottom of station

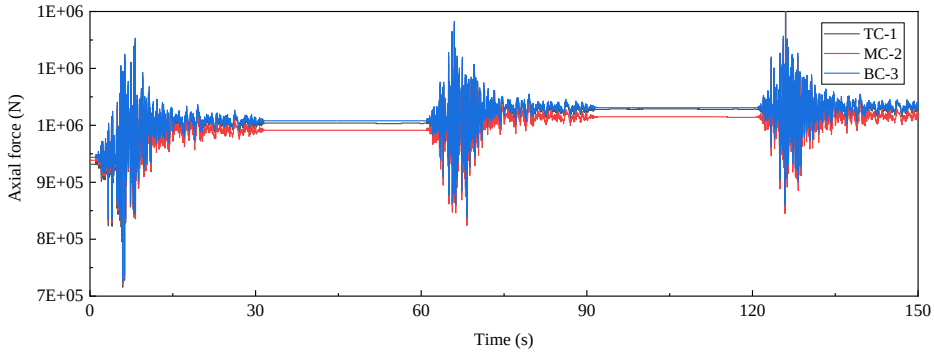

(c) Middle column

Fig. 5 Axial force of station under seismic precautionary intensity of Grade 7

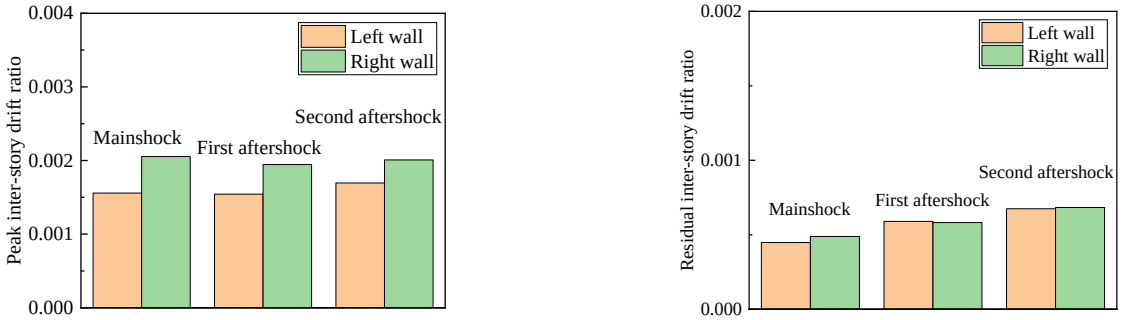

(a) Peak inter-story drift ratio (b) Residual inter-story drift ratio

Fig. 6 Inter-story drift ratio of side wall under the seismic precautionary intensity of Grade 7

Fig. 8 illustrates the peak inter-story drift ratio and residual inter-story drift ratio of side wall with the seismic precautionary intensity of Grade 8. In the three stages of the mainshock-aftershocks, the peak inter-story drift ratio and residual inter-story drift ratio of the left and right side walls show a trend of increase. In the stage of the mainshock,

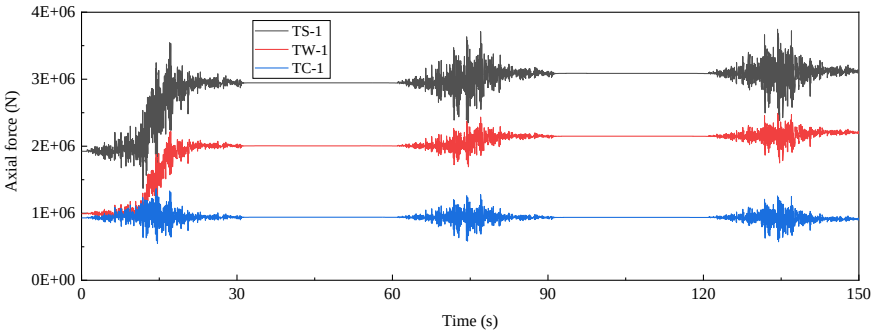

(a) Top of station

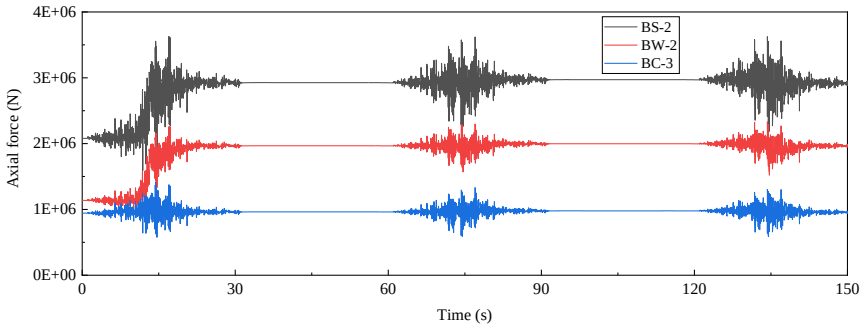

(b) Bottom of station

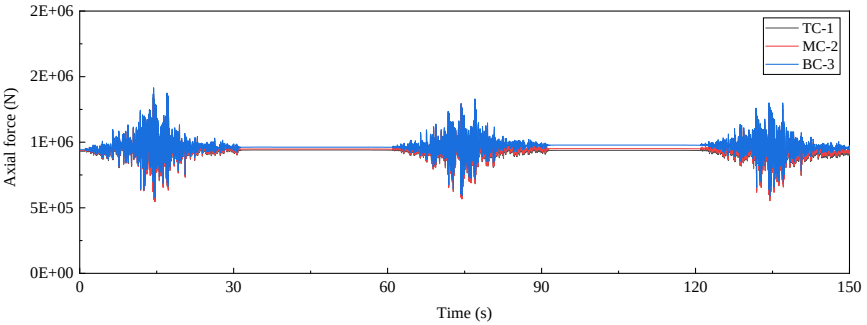

(c) Middle column

Fig. 7 Axial force of station under seismic precautionary intensity of Grade 8

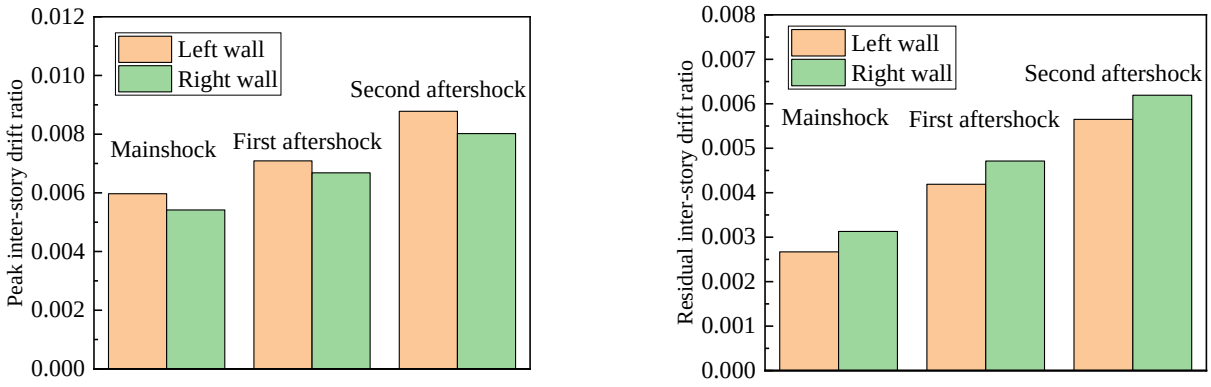

(a) Peak inter-story drift ratio (b) Residual inter-story drift ratio

Fig. 8 Inter-story drift ratio of side wall under the seismic precautionary intensity of Grade 8

although the peak inter-story drift ratio of the station is close to 0.006, the elastic deformation of the station is restored and the inter-story drift ratio decreases after the mainshock. This phenomenon also occurs in the stage of two aftershocks. Under the seismic precautionary intensity of Grade 8, the middle column suffers more damage, especially at the top and bottom. Different from the results under seismic precautionary intensity of Grade 7, two aftershocks cause incremental damage to the structure.

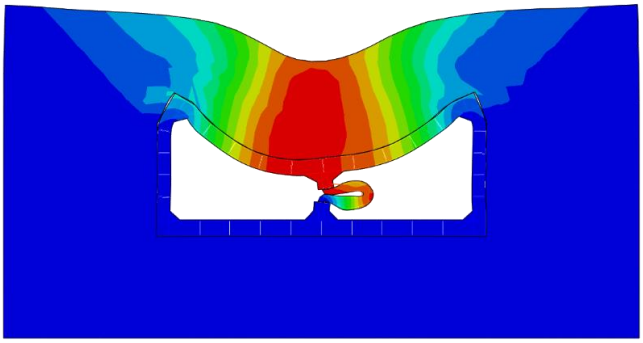

(a) Structure collapse

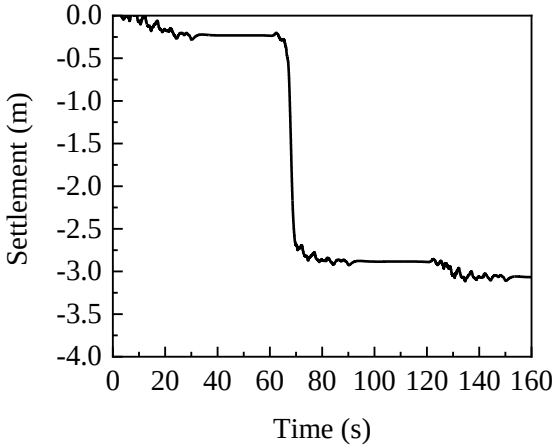

(b) Soil settlement

Fig. 9 Soil settlement at the top of the station

4.3 Seismic precautionary intensity of Grade 9

As shown in Fig. 9, under the seismic precautionary intensity of Grade 9, the middle column of the station is broken and the station is completely collapsed. The final surface settlement is about 3.1 m, and the top of the side wall is separated from the soil. As shown in Fig. 10, compared with the static state, the axial force of the middle column decreases by about 59% after the mainshock. Vertical carrying capacity of the middle column decreases sharply. The vertical load is transferred from the middle column to the side wall. Side wall comes to be the main carrying capacity member, for the proportion of vertical load borne by the side wall increases from 52% to 85%. The axial force of the station increases by about 24%, which is mainly due to the shear failure of the overlying soil. The earth pressure on the structure significantly increases the vertical load of the ceiling, which further leads to the decline in capacity of lateral deformation. In the stage of first aftershock, the carrying capacity of the middle column is further reduced. The inclined column is damaged for the eccentric compression and the carrying capacity of the column is reduced by 75% at 68s. The middle column breaks in the middle and the station collapses.

Fig. 11 shows the variations of the earth pressure with the depth of the subway station before, during and after the earthquake. Before the earthquake, the earth pressure increases linearly with the depth. However, when the station is damaged, the earth pressure at the top of the side wall is almost zero, indicating that the side wall is separated from the soil. The earth pressure at the bottom of the side wall increases, indicating that the stress redistribution has occurred in the station under the action of mainshock-aftershocks, and this phenomenon still exists after the mainshock-aftershocks.

Fig. 12 shows the peak inter-story drift ratio and residual inter-story drift ratio of the station during the mainshock-aftershocks. The inter-story drift ratio in the mainshock is close to 0.01. In the stage of two aftershocks, both the peak inter-story drift ratio and residual inter-story drift ratio are increasing, the maximum peak inter-story drift ratio is about 0.13, and the maximum residual inter-story drift ratio is about 0.129, indicating that the side wall is in a state of plastic failure and irrecoverable deformation occurs. The above analysis shows that under the seismic precautionary intensity of Grade 9, the middle column loses its carrying capacity after mainshock, and the two aftershocks can cause serious incremental damage to the structure, resulting in the collapse of the station.

4.4 Incremental damage

In order to quantitatively describe the damage of the station during the mainshock-aftershocks, the grayscale image binarization is adopted. The damage state of the station can be quantitatively described by calculating the

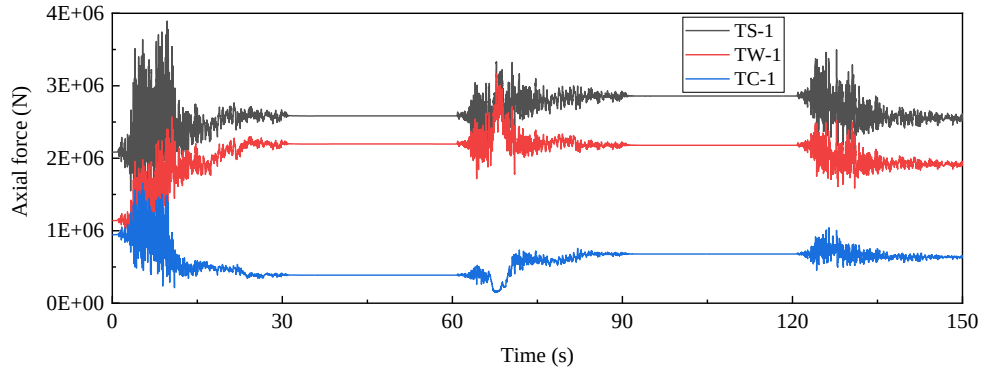

(a) Top of station

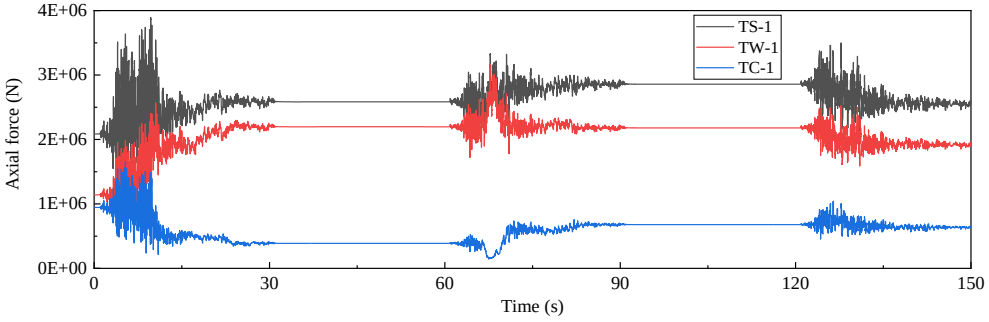

(b) Bottom of station

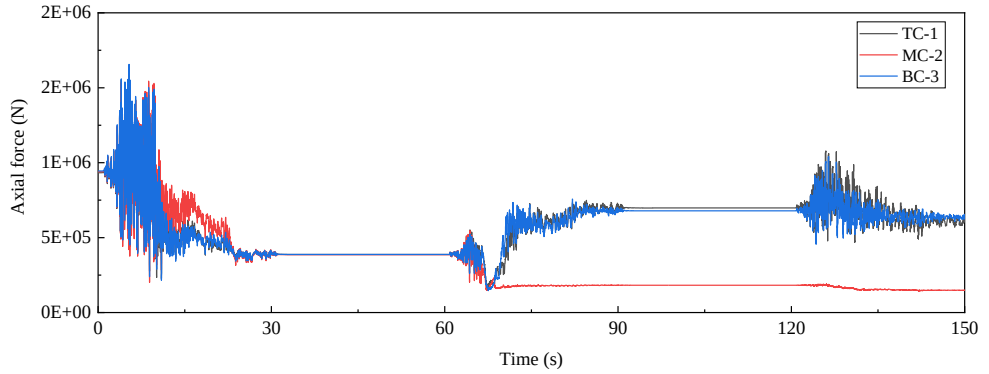

(c) Middle column

Fig. 10 Axial force of station structure under seismic precautionary intensity of Grade 9

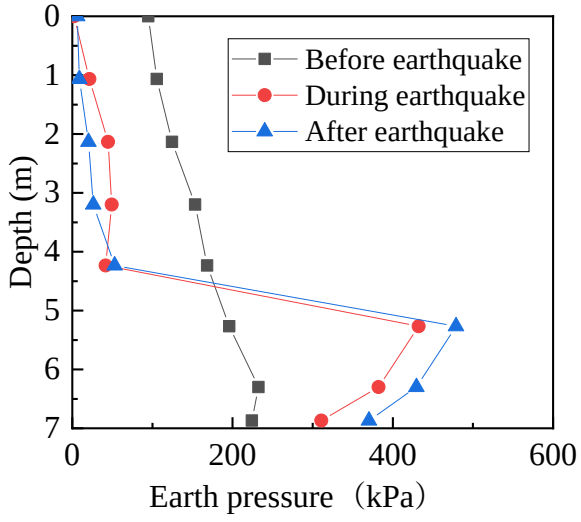

Fig. 11 Variations of the earth pressure with the depth of the subway station

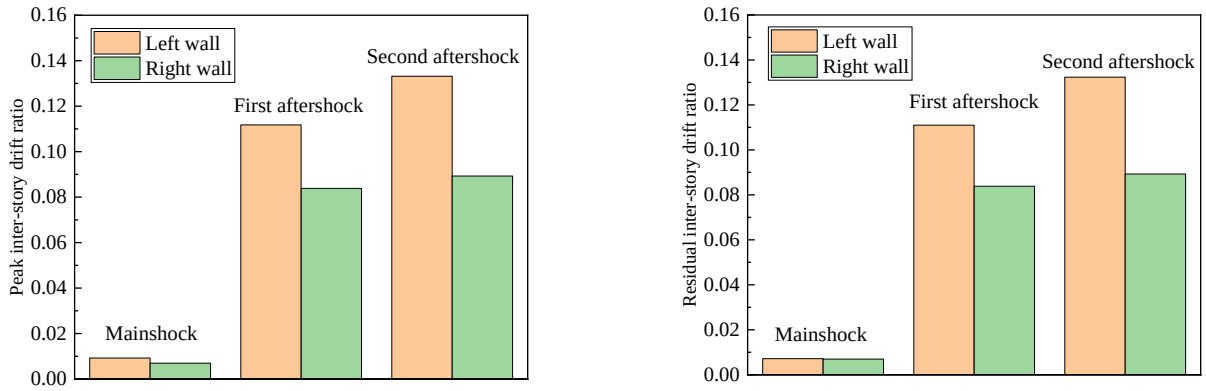

(a) Peak inter-story drift ratio (b) Residual inter-story drift ratio

Fig. 12 Inter-story drift ratio of side wall under the seismic precautionary intensity of Grade 9

Fig. 13 Grayscale image binarization processing

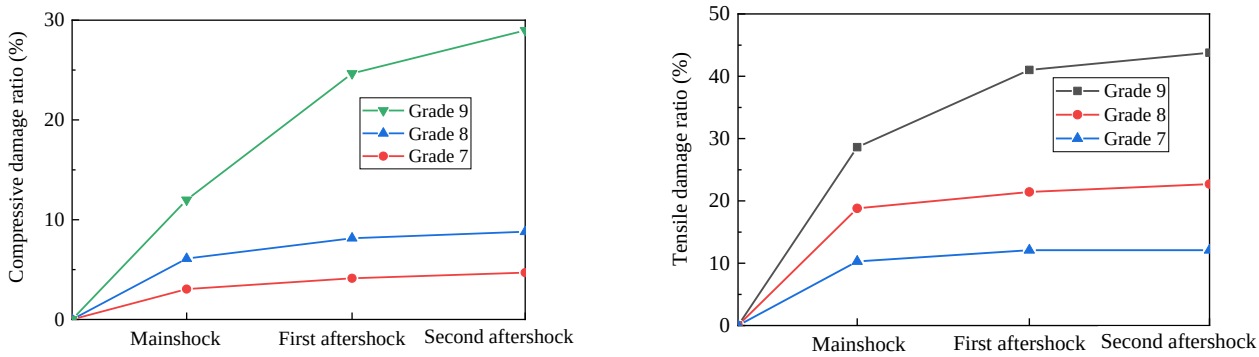

(a) Compressive damage ratio (b) Tensile damage ratio

Fig. 14 Damage ratio of mainshock-aftershocks

damaged area. The color image is composed of R, G and B. The gray image is to calculate the mean value of the pixels of the three colors in the image lattice, and then the gray image is binarized, that is, the pixel value of each lattice of the grayscale image is set to 0 (black) or 255 (white) to make the image black or white. Grayscale image binarization is an important method in the digital image processing.

As shown in Fig. 13, the damage nephogram of the station is binarized by setting the threshold. The black area is intact while the white area is damaged. By calculating the damaged area, the damage condition of the station can be described quantitatively.

For this reason, the concept of incremental damage ratio is introduced, and the damage area after mainshock is defined as D_M; the damage area after aftershock is defined as D_A; the cross-sectional area of station is defined as S; the incremental damage is D_A-D_M; the damage ratio is defined as $\frac{D}{S}$ and incremental damage ratio is defined as $\frac{D_A\text{-}D_M}{D_A}$.

Fig.14 shows the variations of the damage ratio of the station with the seismic precautionary intensity under the tension and the compression, respectively. For the seismic precautionary intensity below Grade 8, the increase of the compression damage ratio is relatively small. The aftershocks almost do not lead to the increase of compression damage ratio of the station. However, for the seismic precautionary intensity of Grade 9, the damage ratio of the structure increases greatly. The tensile damage ratio reaches 43.5% and the station is damaged. When the magnitude of the mainshock and the corresponding aftershock is small and the damage to the structure is slight. The damage ratio of the mainshock under the seismic precautionary intensity of Grade 9 is greater than that of Grade 8, which shows that the magnitude of the mainshock plays a key role to the damage of the station. The stronger the mainshock is, the greater the incremental damage caused by the aftershocks is, which shows that the incremental damage to the station is closely related to the magnitude of the mainshock

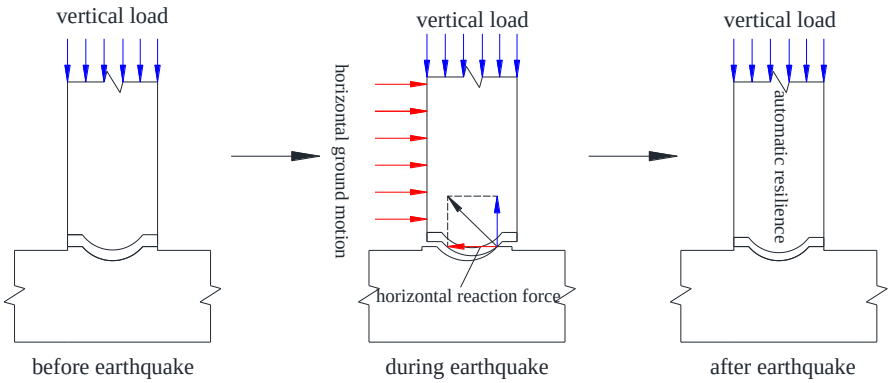

Fig. 15 Schematic diagram of self resetting of arc rubber bearing after horizontal ground motion

5. Damping technology of subway station

The dynamic response analysis of subway station under the action of mainshock-aftershocks shows that the subway station is easy to be destroyed under the action of horizontal shear. The seismic performance of underground structure is weak, especially under the high seismic precautionary intensity. The main reason for the damage to the station is the lack of anti-deformation capacity of the middle column. In order to improve the seismic performance of the underground structure, the deformation coordination ability of the middle column must be enhanced. In this paper, a damping technology of arc rubber bearing is proposed, which can realize the transformation from "fixed connection" to "hinged connection" by changing the traditional connection mode at the bottom of column. The damping technology results in the reduction of the shear force and bending moment at the bottom of column, which avoids the shear failure.

The damping bearing is characteristics of absorbing energy, bearing vertical load, horizontal deformation and self-reset, which can ensure the reliability and safety of the structure to meet the design requirements after the earthquake. The damping technologies include the sliding bearing, the lead rubber bearing, the friction pendulum bearing, the ordinary plate bearing, the ordinary laminated rubber bearing, the bi-directional RFPS bearing, the spherical rubber bearing and so on. (Castaldo *et al*. 2015, Chen and Jia 2021, Chen *et al*. 2021, He and Chen 2021, Jing *et al*. 2021, Ma *et al*. 2022, Zhuang *et al*. 2020) Compared with other damping bearings, the arc rubber bearing proposed in this paper can achieve self-reset function. Under the action of horizontal ground motion, the arc rubber bearing experience the horizontal displacement, and the horizontal cap at both ends of the bearing can avoid the rotation of the middle column around the curved bearing. The horizontal translation displacement of the middle column results in the horizontal reaction force, as shown in Fig. 15. Under the horizontal reaction force, the middle column can reset itself after the earthquake and return to its original stable state in time.

The arc rubber bearing is high damping rubber bearing, which is made of high damping rubber material and laminated steel plate. The bearing does not need to add the lead core, and the change of damping results from the adjustment of the proportion of rubber, which has the capacity of strong ductility and energy dissipation. Arc rubber bearing can decrease the damage of the earthquake to the structure, and the damping effect is remarkable. Rubber is a kind of hyperelastic material, and its mechanical properties are usually described by the elastic potential energy function. In this paper, the Mooney-Rivlin model is adopted, which is a kind of polynomial model.

According to the numerical simulation results of Section 4, the subway station experiences the most serious damage under the seismic precautionary intensity of Grade 9, so the Kobe wave is used as the input ground motion.

From Fig. 16, due to the gravity of the station itself, the axial force of the middle column and side wall at the bottom of the station is slightly higher than that at the top. At 30 s of the mainshock stage, the axial force of the middle column is about double that in the initial state. It is due to the shear failure of the overlying soil, which increases the pressure of the station. However, in the following stages of two aftershock, when the station structure returns to equilibrium, its axial force almost does not increase, indicating that the arc rubber bearing has a good damping performance.

Fig. 16(c) shows the axial force of the middle column after adding the damping bearing. After setting the rubber bearing, the axial force sharing ratio of the middle column and the side wall changes greatly, and the axial force of the middle column in the static state is 40% less than that before shock absorption. The middle column bears 14% of the vertical load, which is 34% lower than that before shock absorption. Part of the vertical load is transferred from the middle column to the side wall. For concrete members, the larger the axial compression ratio is, the weaker the lateral deformation capacity is and the easier it is to be destroyed. Therefore, the lateral deformation capacity of the middle column is well improved by properly reducing the axial compression ratio.

Fig. 17 shows the change of the inter-story drift ratio of the side wall after adding the damping bearing. The peak inter-story drift ratio and residual inter-story drift ratio of the left and right side wall increase in the three stages of the mainshock-

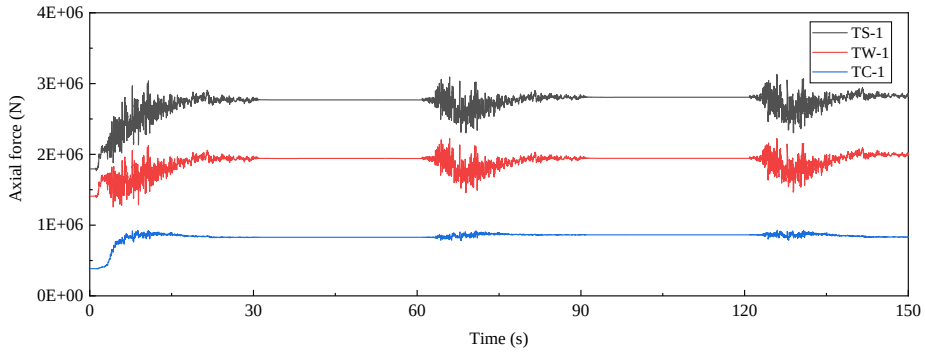

(a) Top of station

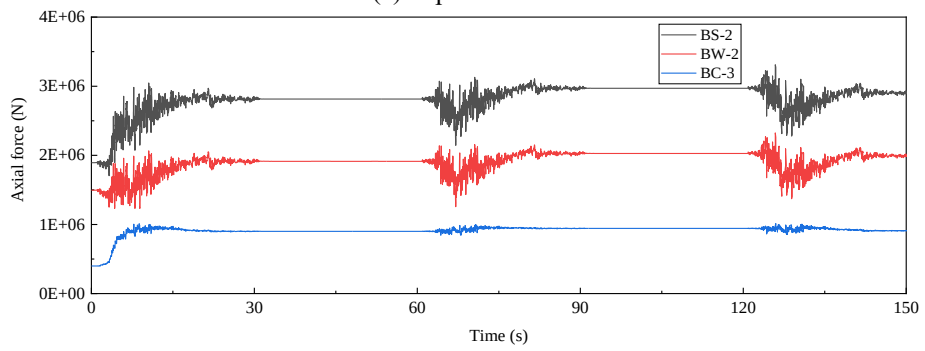

(b) Bottom of station

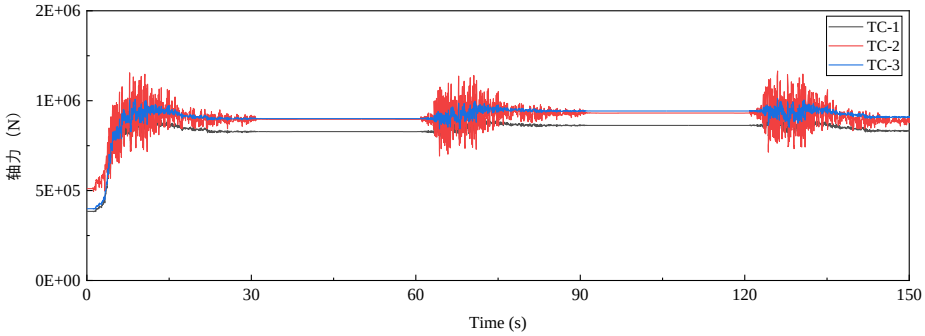

(c) Middle column

Fig. 16 Axial force of station after adding damping bearing

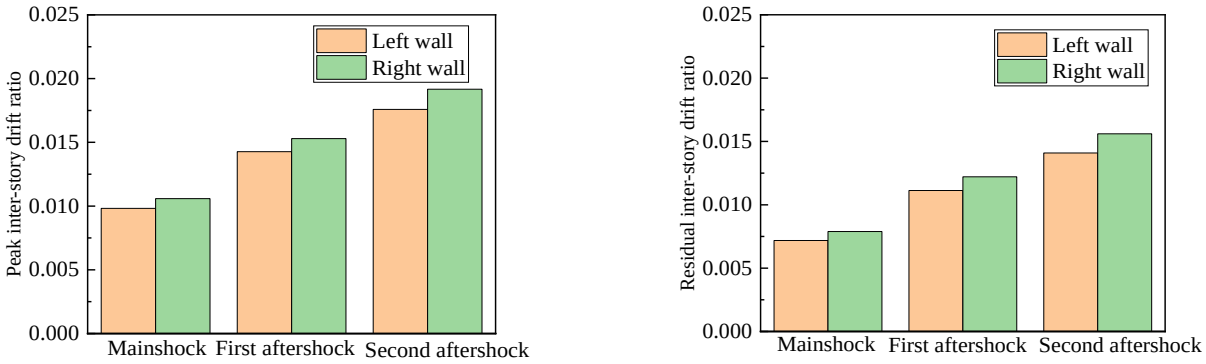

(a) Peak inter-story drift ratio (b) Residual inter-story drift ratio

Fig. 17 Inter-story drift ratio of station after setting damping bearing

aftershocks, mainly because the middle column no longer bears the shear force. The horizontal shear strength of the station decreases, and most of the shear force is borne by the side wall, so the deformation of the side wall is large, but it is still much smaller than that of the station without the damping bearing.

As shown in Fig.18, the compression damage and tensile damage of the station are well improved after adding the

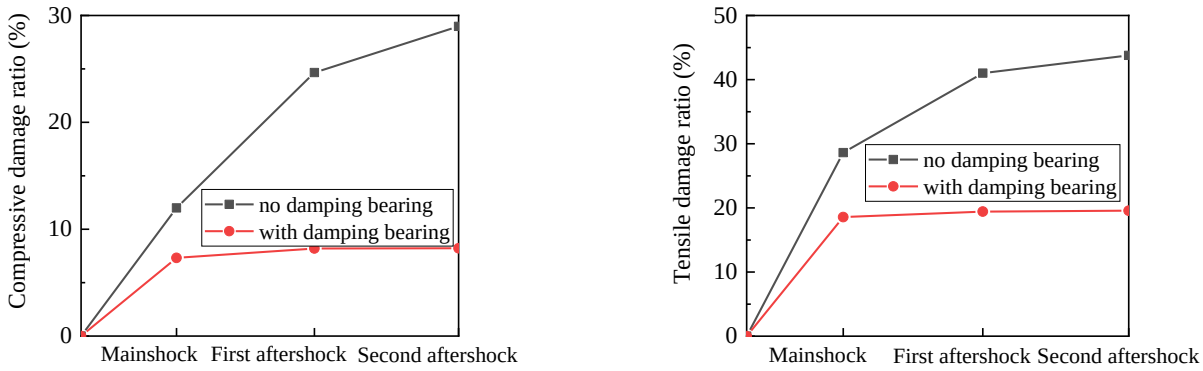

(a) Compressive damage ratio (b) Tensile damage ratio

Fig. 18 Mainshock-aftershocks damage ratio after setting damping bearing

damping bearing. Compared with the traditional station, the tensile damage ratio of the station with the damping bearing under the mainshock is reduced by 10.06%. After adding the damping bearing, the compression and tension damage ratio of the station is only increased by 1% in the stages of two aftershocks. Therefore, the installation of damping bearing greatly reduces the incremental damage of the structure caused by aftershocks, which shows that the arc rubber bearing is effective on the earthquake resistance of the subway station.

6. Conclusions

In this paper, the finite element simulation was used to study the collapse failure mechanism of subway station under the action of mainshock-aftershocks. Firstly, the repetition method was used to construct the mainshock-aftershocks sequence, and then the damage to underground structure under different seismic precautionary intensities was studied based on numerical simulation, which revealed the failure law of subway station under the action of mainshock-aftershocks sequence. Lastly, an arc rubber bearing was proposed for shock absorption and its reliability was verified by numerical simulation. The main conclusions are as follows.

(1) In general, the mainshock plays a most important part in the damage to the structure, and the aftershocks which are closely related to the magnitude of the mainshock can cause the incremental damage to the underground structure. When the magnitude of the mainshock is small, the incremental damage caused by the aftershocks to the structure is less. When the magnitude of the mainshock is high, the incremental damage caused by the aftershocks to the structure is large, and the aftershocks may even lead to the collapse of the station.

(2) In the areas of low seismic precautionary intensity, the aftershocks which have little influence on the incremental damage of the structure could not be considered. However, in the areas of high seismic precautionary intensity, the damage of the structure under the strong mainshock is serious, and the corresponding strong aftershocks will lead to further damage to the station.

(3) An arc rubber bearing improves the stress state of the middle column, transfers the displacement of the column end to the bearing, increases the ductility of the structure, and avoids the shear failure and eccentric compression failure. After the shock absorption, the tensile damage ratio of the structure under the mainshock is reduced by 10.06%, and two aftershocks do not cause the obvious incremental damage to the structure, which effectively avoids the collapse of the station.

Acknowledgements

The work in this paper was funded by National Natural Science Foundation of China (Grant No. 52378381) and National Key Research and Development Program (Grant No. 2017YFC1500702).

References

Amadio, C., Fragiacomo, M. and Rajgelj, S. (2003), "The effects of repeated earthquake ground motions on the non-linear response of SDOF systems", *Earthq. Eng. Struct. D.*, **32**(2), 291-308. https://doi.org/10.1002/eqe.225.

Castaldo, P., Palazzo, B. and Della Vecchia, P. (2015), "Seismic reliability of base-isolated structures with friction pendulum bearings", *Eng. Struct.*, **95**, 80-93. https://doi.org/10.1016/j.engstruct.2015.03.053.

Chen, Z. and Jia, P. (2021), "Seismic response of underground stations with friction pendulum bearings under horizontal and vertical ground motions", *Soil Dyn. Earthq. Eng.*, **151**. https://doi.org/10.1016/j.soildyn.2021.106984.

Chen, Z., Jia, P., Fan, Y. and Liu, Z. (2021), "Parameter analysis and optimization of friction pendulum bearings in underground stations based on genetic algorithm", *J. Earthq. Eng.*, **26**(15), 7814-7831. https://doi.org/10.1080/13632469.2021.1988765.

Chou, J.C. and Lin, E.G.E. (2020), "Incorporating ground motion effects into Sasaki and Tamura prediction equations of liquefaction-induced uplift of underground structures", *Geomech. Eng.*, **22**(1), 25-33. https://doi.org/10.12989/gae.2020.22.1.025.

Cui, Z.D., Huang, M.H., Hou, C.Y. and Yuan, L. (2023a), "Seismic deformation behaviors of the soft clay after freezing-thawing", *Geomech. Eng.*, **34**(3), 303-316. https://doi.org/10.12989/gae.2023.34.3.303.

Cui, Z.D., Zhang, L.J. and Zhan, Z.X. (2023b), "Dynamic shear modulus and damping ratio of saturated soft clay under the seismic loading", *Geomech. Eng.*, **32**(4), 411-426.

https://doi.org/10.12989/gae.2023.32.4.411.

Hatzigeorgiou, G.D. and Beskos, D.E. (2009), "Inelastic displacement ratios for SDOF structures subjected to repeated earthquakes", *Eng. Struct.*, **31**(11), 2744-2755. https://doi.org/10.1016/j.engstruct.2009.07.002.

He, Z. and Chen, Q. (2021), "Upgrading the seismic performance of underground structures by introducing lead-filled steel tube dampers", *Tunn. Undergr. Sp. Tech.*, **108**. https://doi.org/10.1016/j.tust.2020.103727.

Huynh, V.Q., Nguyen, T.K. and Nguyen, X.H. (2021), "Seismic analysis of soil-structure interaction: Experimentation and modeling", *Geomech. Eng.*, **27**(2), 115-121. https://doi.org/10.12989/gae.2021.27.2.115.

Jing, Y., Haiyang, Z., Wei, W., Zhenghua, Z. and Guoxing, C. (2021), "Seismic performance and effective isolation of a large multilayered underground subway station", *Soil Dyn. Earthq. Eng.*, **142**. https://doi.org/10.1016/j.soildyn.2020.106560.

Kim, B. and Shin, M. (2017), "A model for estimating horizontal aftershock ground motions for active crustal regions", *Soil Dyn. Earthq. Eng.*, **92**, 165-175. https://doi.org/10.1016/j.soildyn.2016.09.040.

Kim, Y., Lim, H. and Jeong, S. (2020), "Seismic response of vertical shafts in multi-layered soil using dynamic and pseudo-static analyses", *Geomech. Eng.*, **21**(3), 269-277. https://doi.org/10.12989/gae.2020.21.3.269.

Kirkwood, P. and Dashti, S. (2018a), "A centrifuge study of seismic structure-soil-structure interaction on liquefiable ground and implications for design in dense urban areas", *Earthq. Spectra*, **34**(3), 1113-1134. https://doi.org/10.1193/052417eqs095m.

Kirkwood, P. and Dashti, S. (2018b), "Considerations for the Mitigation of Earthquake-Induced Soil Liquefaction in Urban Environments", *J. Geotech. Geoenviron. Eng.*, **144**(10). https://doi.org/10.1061/(asce)gt.1943-5606.0001936.

Kwon, S.Y., Yoo, M. and Hong, S. (2020), "Earthquake risk assessment of underground railway station by fragility analysis based on numerical simulation", *Geomech. Eng.*, **21**(2), 143-152. https://doi.org/10.12989/gae.2020.21.2.143.

Lu, C.C. and Hwang, J.H. (2018), "Damage analysis of the new Sanyi railway tunnel in the 1999 Chi-Chi earthquake: Necessity of second lining reinforcement", *Tunn. Undergr. Sp. Tech.*, **73**, 48-59. https://doi.org/10.1016/j.tust.2017.12.009.

Ma, C., Lu, D., Zhao, Y., Wang, Z. and Du, X. (2022), "Performance of an underground structure seismic mitigation system improved by frictional deformation absorbing braces", *Structures*, **37**, 1-16. https://doi.org/10.1016/j.istruc.2021.12.082.

Moustafa, A. and Takewaki, I. (2010), "Modeling critical ground-motion sequences for inelastic structures", *Adv. Struct. Eng.*, **13**(4), 665-679. https://doi.org/10.1260/1369-4332.13.4.665.

Ruiz-Garcia, J. (2012), "Mainshock-aftershock ground motion features and their influence in building's seismic response", *J. Earthq. Eng.*, **16**(5), 719-737. https://doi.org/10.1080/13632469.2012.663154.

Sudevan, P.B., Boominathan, A. and Banerjee, S. (2020), "Mitigation of liquefaction-induced uplift of underground structures by soil replacement methods", *Geomech. Eng.*, **23**(4), 365-379. https://doi.org/10.12989/gae.2020.23.4.365.

Tsinidis, G. (2017). "Response characteristics of rectangular tunnels in soft soil subjected to transversal ground shaking", *Tunn. Undergr. Sp. Tech.*, **62**, 1-22. https://doi.org/10.1016/j.tust.2016.11.003.

Wang, W.L., Wang, T.T., Su, J.J., Lin, C.H., Seng, C.R. and Huang, T.H. (2001). "Assessment of damage in mountain tunnels due to the Taiwan Chi-Chi Earthquake", *Tunn. Undergr. Sp. Tech.*, **16**(3), 133-150. https://doi.org/10.1016/s0886-7798(01)00047-5.

Wang, Z., Gao, B., Jiang, Y. and Yuan, S. (2009), "Investigation and assessment on mountain tunnels and geotechnical damage after the Wenchuan earthquake", *Science in China Series E-Tech. Sci.*, **52**(2), 546-558. https://doi.org/10.1007/s11431-009-0054-z.

Xu, C., Zhang, Z., Li, Y. and Du, X. (2020a), "Validation of a numerical model based on dynamic centrifuge tests and studies on the earthquake damage mechanism of underground frame structures", *Tunn. Undergr. Sp. Tech.*, **104**. https://doi.org/10.1016/j.tust.2020.103538.

Xu, Z., Du, X., Xu, C. and Han, R., (2020b), "Numerical analyses of seismic performance of underground and aboveground structures with friction pendulum bearings", *Soil Dyn. Earthq. Eng.*, **130**. https://doi.org/10.1016/j.soildyn.2019.105967.

Xu, Z., Du, X., Xu, C., Hao, H., Bi, K. and Jiang, J. (2019), "Numerical research on seismic response characteristics of shallow buried rectangular underground structure", *Soil Dyn. Earthq. Eng.*, **116**, 242-252. https://doi.org/10.1016/j.soildyn.2018.10.030.

Yin, Y.J. and Li, Y. (2011), "Loss estimation of light-frame wood construction subjected to mainshock-aftershock sequences", *J. Perform. Constr. Fac.*, **25**(6), 504-513. https://doi.org/10.1061/(asce)cf.1943-5509.0000187.

Yoo, M., Kwon, S.Y. and Hong, S. (2022), "Dynamic response evaluation of deep underground structures based on numerical simulation", *Geomech. Eng.*, **29**(3), 269-279. https://doi.org/10.12989/gae.2022.29.3.269.

Yu, X.H., Li, S., Lu, D.G. and Tao, J. (2020), "Collapse capacity of inelastic single-degree-of-freedom systems subjected to mainshock-aftershock earthquake sequences", *J. Earthq. Eng.*, **24**(5), 803-826. https://doi.org/10.1080/13632469.2018.1453417.

Zhuang, H., Zhao, C., Chen, S., Fu, J., Zhao, K. and Chen, G. (2020), "Seismic performance of underground subway station with sliding between column and longitudinal beam", *Tunn. Undergr. Sp. Tech.*, **102**. https://doi.org/10.1016/j.tust.2020.103439.

GC